Monthly Notices of the ROYAL ASTRONOMICAL SOCIETY

MNRAS **480,** 2411–2422 (2018) doi:10.1093/mnras/sty1933
Advance Access publication 2018 July 19

The first super-Earth detection from the high cadence and high radial velocity precision Dharma Planet Survey

Bo Ma,[1]★ Jian Ge,[1] Matthew Muterspaugh,[2,3] Michael A. Singer,[1] Gregory W. Henry,[3] Jonay I. González Hernández,[4,5] Sirinrat Sithajan,[1] Sarik Jeram,[1] Michael Williamson,[3] Keivan Stassun,[6] Benjamin Kimock,[1] Frank Varosi,[1] Sidney Schofield,[1] Jian Liu,[1] Scott Powell,[1] Anthony Cassette,[1] Hali Jakeman,[1] Louis Avner,[1] Nolan Grieves,[1] Rory Barnes,[7] Bo Zhao,[1] Sankalp Gilda,[1] Jim Grantham,[8] Greg Stafford,[8] David Savage,[8] Steve Bland[8] and Brent Ealey[8]

[1]*Department of Astronomy, University of Florida, 211 Bryant Space Science Center, Gainesville, FL 32611-2055, USA*
[2]*Department of Mathematics and Physics, College of Life and Physical Sciences, Tennessee State University, Boswell Science Hall, Nashville, TN 37209, USA*
[3]*Tennessee State University, Center of Excellence in Information Systems, Nashville, TN 37203, USA*
[4]*Instituto de Astrofísica de Canarias, C/Vía Láctea S/N, E-38200 La Laguna, Spain*
[5]*Departamento de Astrofísica, Universidad de La Laguna, E-38205 La Laguna, Tenerife, Spain*
[6]*Department of Physics & Astronomy, Vanderbilt University, Nashville, TN 37235 USA*
[7]*Astronomy Department, University of Washington, Box 951580, Seattle, WA 98195, USA*
[8]*Steward Observatory, The University of Arizona, Tucson, AZ 85719, USA*

Accepted 2018 July 18. Received 2018 July 3; in original form 2018 April 5

ABSTRACT

The Dharma Planet Survey (DPS) aims to monitor about 150 nearby very bright FGKM dwarfs (within 50 pc) during 2016–2020 for low-mass planet detection and characterization using the TOU very high resolution optical spectrograph ($R \approx 100\,000$, 380–900 nm). TOU was initially mounted to the 2-m Automatic Spectroscopic Telescope at Fairborn Observatory in 2013–2015 to conduct a pilot survey, then moved to the dedicated 50-inch automatic telescope on Mt. Lemmon in 2016 to launch the survey. Here, we report the first planet detection from DPS, a super-Earth candidate orbiting a bright K dwarf star, HD 26965. It is the second brightest star ($V = 4.4$ mag) on the sky with a super-Earth candidate. The planet candidate has a mass of $8.47 \pm 0.47 M_{\rm Earth}$, period of 42.38 ± 0.01 d, and eccentricity of $0.04^{+0.05}_{-0.03}$. This radial velocity (RV) signal was independently detected by Díaz et al., but they could not confirm if the signal is from a planet or stellar activity. The orbital period of the planet is close to the rotation period of the star (39–44.5 d) measured from stellar activity indicators. Our high precision photometric campaign and line bisector analysis of this star do not find any significant variations at the orbital period. Stellar RV jitters modelled from star-spots and convection inhibition are also not strong enough to explain the RV signal detected. After further comparing RV data from the star's active magnetic phase and quiet magnetic phase, we conclude that the RV signal is due to planetary-reflex motion and not stellar activity.

Key words: techniques: photometric – techniques: radial velocities – techniques: spectroscopic – planets and satellite: detection.

1 INTRODUCTION

Results emerging from the *Kepler* mission and ground-based radial velocity (RV) surveys reveal a population of close-in low-mass planets orbiting FGKM stars (Howard et al. 2010, 2012; Mayor et al. 2011; Bonfils et al. 2013). Most of these low-mass planets have orbital periods shorter than the 88-d orbit of Mercury, and many of them are in very compact multiple-planet systems (e.g. Howard et al. 2012; Batalha et al. 2013; Mullally et al. 2015; Coughlin et al. 2016; Morton et al. 2016). This unexpected population of close-in low-mass planets (super-Earths and Neptune-mass planets), which is completely absent in our own Solar system, is surprisingly common

★ E-mail: xiaomabo@gmail.com, boma@ufl.edu

and represents the most dominant class of planetary systems known to date. However, the measured occurrence rate of this close-in low-mass planet population varies significantly between different RV groups, ranging from ∼23 per cent to 50 per cent (Howard et al. 2010; Mayor et al. 2011; Bonfils et al. 2013). The large uncertainties in the ground-based RV survey results are largely due to their low-cadence survey strategy. For instance, the average number of RV measurements per survey target is between 20 and 40, and they were typically spread out over six years (Howard et al. 2010; Mayor et al. 2011; Bonfils et al. 2013; Motalebi et al. 2015; Borgniet et al. 2017; Perger et al. 2017).

Kepler has enabled estimates of the occurrence rates of low-mass planets with orbits as long as 300 d (e.g. Petigura, Marcy & Howard 2013; Foreman-Mackey, Hogg & Morton 2014; Burke et al. 2015). However, the uncertainties in the *Kepler* measurements remain large due to the unknown false positive rate, and systematic errors caused by *Kepler*'s pipeline completeness, survey selection effects, and catalogue reliability (Burke et al. 2015; Christiansen et al. 2016). For instance, the estimated false positive rate is ∼11 per cent for low-mass planet candidates (Fressin et al. 2013) and ∼55 per cent for giant planet candidates (Santerne et al. 2016). The systematic errors in candidate detection have led to a factor of 2–3 times difference in estimates of the occurrence rates of low-mass exoplanets from different transiting groups (e.g. Howard et al. 2012; Petigura et al. 2013; Foreman-Mackey et al. 2014; Dressing & Charbonneau 2015; Burke et al. 2015; Mulders, Pascucci & Apai 2015). In addition, due to strict edge-on geometry requirements, *Kepler* may have missed some non-transiting planets in the *Kepler* transit planet systems, leading to additional uncertainties in the occurrence rate measurements (e.g. Buchhave et al. 2016).

It is quite clear that an independent and uniform measurement of the occurrence rate of this close-in small planet population is necessary. This independent survey will not only help address the discrepancies between previous surveys and constrain planet formation theories, but also help independently resolve controversial low-mass planet discovery claims by different RV surveys using different RV instruments, or different data pipelines using the same instrument. For example, two groups reported four (Mayor et al. 2009) and six (Vogt et al. 2010) low-mass planets orbiting GJ 581, respectively. The same two groups reported six planets (Vogt et al. 2015) and four planets (Motalebi et al. 2015) orbiting HD 219134, respectively. These uncertainties greatly affect our understanding of exoplanet systems and their architectures, especially those with low-mass planets. More independent observations from high-precision RV campaigns are required to resolve these debates.

High cadence and high RV precision observation of survey stars can significantly improve sensitivity for detecting close-in low-mass planets. It is very challenging to search for close-in low-mass planets which produce very small RV signals over 1–2 month periods, as previous RV surveys on large telescopes (such as Keck and High Accuracy Radial velocity Planet Searcher (HARPS)) often suffer from sparse and irregular observation cadences due to sharing requirements. For example, Anglada-Escudé et al. (2016) pointed out that uneven and sparse sampling is one of the reasons why Proxima b could not be unambiguously confirmed with their pre-2016 RV data. This likely accounted for the large discrepancy in low-mass planet occurrence rates by different groups (Howard et al. 2010; Mayor et al. 2011). Continuous phase coverage with high RV precision would likely remove these discrepancies. Pioneering observations by HARPS of 10 very stable FGK dwarfs with high cadence (∼50 data points per observing season, and an average of 122 RV points per star) and precision (∼0.9–2.6 $m\,s^{-1}$) led to detection of three low-mass planetary systems with six low-mass planets (one with as low as 3.6 $M_{\oplus}$, Pepe et al. 2011), which otherwise would have largely escaped detection.

The Dharma Planet Survey (DPS) was designed to detect and characterize close-in low-mass planets and sub-Jovian planets. The ultimate survey goal is to detect potentially habitable super-Earth planet candidates and provide bright high-priority follow-up targets for future space missions (such as James Webb SPace Telescope (*JWST*), the Wide Field Infrared Survey Telescope-Astrophysics Focused Telescope Assets (WFIRST-AFTA), Exoplanet direct imaging Coronagraph (EXO-C), xoplanet direct imaging Starshade (EXO-S), and the Large UV/Optical/IR Surveyor (LUVOIR)) to identify possible biomarkers supporting life (Ge et al. 2016). It will initially search for and characterize low-mass planets around 150 nearby very bright FGKM dwarfs in 2016–2020.

The DPS survey, unlike previous and on-going low-mass high-precision RV planet surveys with varying numbers of measurements (from a few RV data points to ∼400 RV data points, e.g. Dumusque et al. 2012), will offer a nearly homogeneous high cadence for every survey target. Every target will be initially observed ∼30 consecutive observable nights to target close-in low-mass planets detection. After that, each target will be observed an additional ∼70 times randomly spread over 420 d. The automatic nature of the 50-inch telescope and its flexible queue observation schedule are key to realizing this nearly homogenous high cadence. This cadence will minimize time-aliasing and RV jitter effects caused by stellar activity that often preclude the detection of low-mass planets, especially those in highly eccentric orbits, which may have been missed by previous surveys (Dumusque et al. 2011; Vanderburg et al. 2016). Because of the high cadence for every survey star, both detections and non-detections from the survey can be reliably used for statistical studies. The proposed survey strategy, cadence, and schedule will therefore offer the optimal accuracy to assess the survey completeness and to determine occurrence rates of low-mass planets. This survey will offer a homogeneous data set for constraining formation models of low-mass planets with periods less than 450 d. In addition, this DPS survey strategy provides an efficient way to explore habitable low-mass planets around nearby FGKM dwarfs with greatly improved survey sensitivity and completeness compared to previous Doppler surveys.

In this paper, we report the first planet detection from DPS survey, a super-Earth candidate orbiting a nearby bright K0.5V star with $V = 4.4$ mag, HD 26965. The RV signal has also been reported recently in Díaz et al. (2018), in which they claim it is either a planet signal, or a signal from stellar activity. In Section 2, we describe the observations used in this paper. We present stellar parameters for the star in Section 3 and orbital parameters for the planet candidate in Section 4. We discuss the nature of the RV signal in Section 5. In Section 6, we discuss our results and present our conclusions.

2 OBSERVATIONS AND RADIAL VELOCITY EXTRACTION

2.1 TOU RV Data

TOU (formerly called EXPERT-III) is a fibre-fed, cross-dispersed echelle spectrograph with a spectral resolution of about 100 000, wavelength coverage of 3800–9000 Å, and a 4k x 4k Fairchild CCD detector (Ge et al. 2012, 2014). The instrument holds a very high vacuum of 1 μTorr and about 1mK temperature stability over a month.

Table 1. RV measurements of HD 26965 from TOU. The entire RV data set is available online only.

FCJD	RV (m s^{-1})	Err (m s^{-1})
2456945.795540	− 3.6	1.4
2456947.791740	− 2.2	1.4
2456948.844430	3.1	1.4
2456950.828580	0.3	2.2
2456951.861620	− 4.4	1.5
2456952.825790	− 3.2	1.3

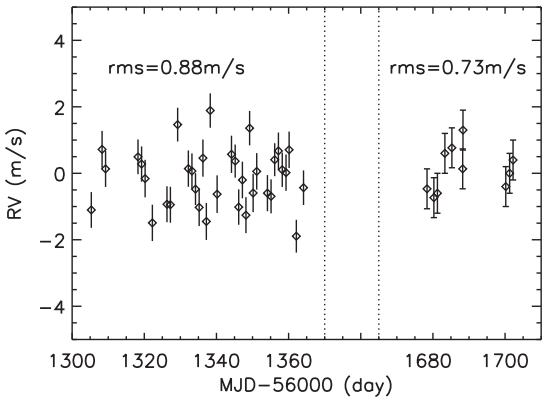

Figure 1. Radial velocity measurements of an RV stable star, HD 10700, from 2015 to 2016. Each data point is obtained by combining three 10 min exposures of the star to remove the short-term stellar oscillation noise. The rms precision is between 0.7 and 0.9 m s^{-1}.

We obtained 66 observations of HD 26965 using TOU at the 2-m Automatic Spectroscopic Telescope (AST) at Fairborn Observatory between 2014 and 2015. We later moved TOU to the UF 50-inch robotic telescope at Mt. Lemmon, called the Dharma Endowment Foundation Telescope (DEFT) . We obtained an additional 67 data points during 2016–2017. The exposure time is chosen to be 10 min to achieve sufficient signal-to-noise ratio (S/N > 100 at 5500 Å). The data are then processed by an IDL-based data reduction pipeline (Ma & Ge in preparation). This pipeline calculates the RV by matching the wavelength calibrated stellar spectra to a stellar template, which is generated by combining all available stellar observations of HD 26965. The RV data are summarized in Table 1.

To demonstrate the RV precision of the TOU spectrograph, we also monitored an RV stable star, HD 10700, and a known planet host star, HD 1461 (Rivera et al. 2010), using TOU between 2015 and 2016. On each night, we obtained three 10 min exposures of HD 10700 and combined them to calculate the RV for HD 10700 on that night. This can help average out the short-term periodic stellar oscillation noise (Dumusque et al. 2011), thus, reducing the RV noise from stellar activity. The RV data for HD 10700 are displayed in Fig. 1, which shows an RV scatter of ∼0.8 m s^{-1}. For HD 1461, we obtained one 30 min exposure on each night. The phased RV curve is displayed in Fig. 2, which shows we have successfully recovered this planet RV signal.

2.2 Keck/HIRES RV Data

The HIRES (Vogt et al. 1994) spectrograph covers a wavelength range of 3700–8000 Å. It uses the iodine cell technique to measure RVs (Butler et al. 1996). Butler et al. (2017) released 20 yr of precision RVs from HIRES on the Keck-I telescope carried out

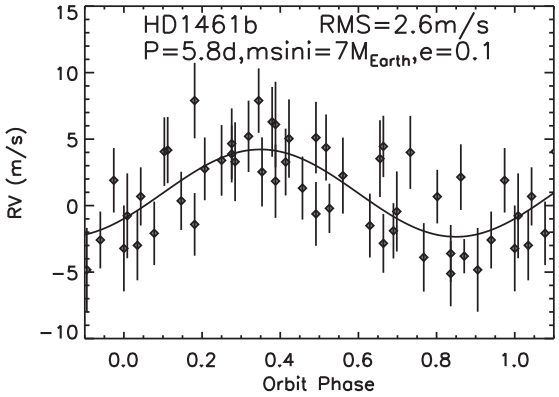

Figure 2. Phase-folded RV curve of HD 1461. The RV measurements are from TOU. The planet has a period of 5.8 d, and eccentricity of 0.1. The best-fitting Keplerian orbital model is also shown, with a residual rms of 2.6 m s^{-1}. These RV observations demonstrate TOU has the ability to detect super-Earths around nearby bright stars.

by the Lick-Carnegie Exoplanet Survey Team. HD 26965 was one of the targets covered by this survey. We found a total of 284 observations for HD 26965 from Butler et al. (2017). We find there exists a ∼30 m s^{-1} offset between the RV data for HD 26965 before and after 2014 August. Such a big RV offset may be triggered by many causes, such as instrument effects, bad wavelength calibration, or data reduction pipeline glitch. Since we can not identify the exact cause for such a big RV offset, we decide to use only the 236 RV data points taken on 92 nights before 2014 August in this study to minimize inconsistency potentially caused by bad RV data products. It is worth pointing out that Díaz et al. (2018) also only use HIRES RV data taken before 2014 August in their paper. The S-indices from Ca II H and K lines derived from Keck/HIRES data are also available from (Butler et al. 2017).

2.3 HARPS RV Data

HARPS is a pressure and temperature stabilized spectrograph, which has a spectral resolving power of $R \sim 115\,000$ and a wavelength range between 3800 and 6300 Å (Mayor et al. 2003). The HARPS data for HD 26965 are downloaded from the European Southern Observatory PHASE3 archive website. We find a total of 483 good exposures on 78 nights from 2003 October to 2015 January, with exposure times ranging between 30 s and 10 min, which are labelled as HARPS old data. HARPS vacuum enclosure was opened in 2015 as part of an upgrade campaign. We include 82 HARPS post-upgrade RV measurements between 2015 September and 2016 March from (Díaz et al. 2018), which are labelled as HARPS new data throughtout this paper. The spectral data are reduced using the standard HARPS Data Reduction Software.

2.4 PFS RV data

The Carnegie Planet Finder Spectrograph (PFS) has spectral resolution of $R \sim 80\,000$, and is equipped with an I_2 cell for precise RV measurements. Spectroscopic observations were carried out using PFS (Crane et al. 2010) between 2011 and 2016. There are a total of 68 individual RV measurements obtained on 20 different nights. The typical S/N ratio is ∼300 per resolution element, which delivers a level of ∼1–2 m s^{-1} RV precision. The PFS RV measurements data and corresponding S-indices are taken from table 8 in Díaz et al. (2018).

2.5 CHIRON RV data

CHIRON is a fibre-fed high-resolution echelle spectrograph with a resolution of $R \sim 95\,000$ using the slit mode and 3×1 pixel binning (Tokovinin et al. 2013). It has a wavelength coverage of 4150–8800 Å. The wavelength calibrated spectra are reduced using a pipeline from Brewer, Giguere & Fischer (2014). The Doppler shifts are calculated using a standard I_2 technique. There are a total of 258 measurements taken on 107 nights, with a median RV error of $\sigma = 1.60$ m s^{-1} . The RV measurements are taken from table 9 in Díaz et al. (2018).

2.6 Photometric observations

We acquired 1550 good photometric observations of HD 26965 during 24 consecutive observing seasons between 1993 September and 2017 February, all with the T4 0.75 m Automatic Photoelectric Telescope (APT) at Fairborn Observatory in the Patagonia Mountains of southern Arizona. The T4 APT is one of several automated telescopes operated at Fairborn by Tennessee State University and is equipped with a single-channel precision photometer that uses an EMI 9924B bi-alkali photomultiplier tube to count photons in the Strömgren *b* and *y* pass bands (Henry et al. 1999). Further information on the operation of our automated telescopes, precision photometers, and observing and data reduction techniques can be found in Henry (1995a,b), Henry et al. (1999), and Eaton, Henry & Fekel (2003).

3 STELLAR PARAMETERS

HD 26965 is the primary of a very widely separated triple system. The other two companions are an M4 dwarf and a white dwarf. The on-sky separation between the primary and the other two stars is about 82 arcsec. The estimated orbital period of this system is ∼8000 yr (Heintz 1974). This star has a star-spot activity cycle period of 10.1 yr (Baliunas et al. 1995).

The stellar parameters are derived from excitation and ionization equilibria of Fe. We first normalize the stellar spectra in each order and merge them into a single spectrum in the spectral range 465–617 nm. We then derive equivalent widths (EWs) of Fe I and Fe II lines with the code TAME (Kang & Lee 2012), using an initial line list with 75 Fe I and 10 Fe II lines from Tsantaki et al. (2013), after discarding Fe lines with EW >120 mÅ and with EW <10 mÅ. The stellar atmospheric parameters are computed using the code STEPAR (Tabernero, Montes & González Hernández 2012), which uses the MOOG code (in its 2014 version, Sneden 1973) and a grid of Kurucz ATLAS9 plane-parallel model atmospheres (Kurucz 1993a). STEPAR iterates until the slopes of A(Fe I) versus χ and A(Fe I) versus log(EW/λ) are equal to zero, while imposing the ionization equilibrium condition A(Fe I) = A(Fe II). STEPAR does a second iteration of the stellar parameter determination after rejecting the Fe lines with an EW and corresponding Fe abundance outliers using a 3σ clipping procedure. 61 Fe I lines and 9 Fe II lines remain after clipping, which produce $T_{\rm eff} = 5072 \pm 53$ K, $\log(g) = 4.45 \pm 0.19$, [Fe/H] $= -0.42 \pm 0.04$. Therefore, HD 26965 is a metal-poor star compared to our Sun. Using the mass–radius–stellar parameters relation from Torres, Andersen & Giménez (2010), we calculate HD 26965 to have a stellar mass of 0.78 $M_\odot$ and a stellar radius of 0.87 $R_\odot$. We listed these parameters in Table 2.

For comparison, the stellar parameters for HD 26965 were also derived from HARPS spectra by Delgado Mena et al. (2017). The abundances were determined from a standard local thermodynamic equilibrium analysis using measured EWs injected into the code MOOG and a grid of Kurucz ATLAS9 atmospheres. They reported $T_{\rm eff} = 5098 \pm 32$ K, $\log(g) = 4.35 \pm 0.10$, and [Fe/H] $= -0.36 \pm 0.02$, which are consistent with our results from our TOU spectra. Díaz et al. (2018) also derived stellar parameters for HD 26965, which agree with our results as well. Therefore, we only report our results from TOU in Table 2.

Table 2. Stellar parameters of HD 26965.

Parameter	Value
Effective temperature	5072 ± 53 K
log(g)	4.45 ± 0.19
[Fe/H]	-0.42 ± 0.04
Spectral type	K0 V
Mass (Torr)	$0.78 \pm 0.08\ M_\odot$
Radius (Torr)	$0.87 \pm 0.17\ R_\odot$
Radius (SED)	$0.812 \pm 0.017\ R_\odot$
$\log(R'_{HK})$	-4.99^a
Age	6.9 ± 4.7 Gyr
A_V	$0.00^{+0.01}_{-0.00}$
F_{bol}	$5.06 \pm 0.12e^{-7}$ erg s^{-1} cm^{-2}
Distance from *Hipparcos*	4.985 ± 0.001 pc

Note: [a]Data from Jenkins et al. (2011).

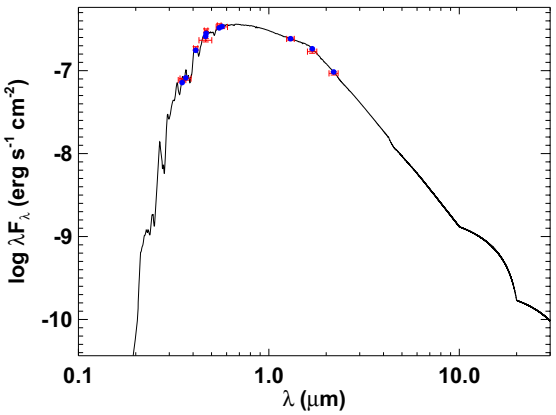

Figure 3. The observed SED from the optical through the IR for HD 26965, along with Kurucz ATLAS model atmosphere. Blue points represent the expected fluxes in each band based on the model, red horizontal bars are the approximate bandpass widths, and red vertical bars are the flux uncertainties.

We also did an SED fitting using Johnson *UBV* (Ducati 2002), Stromgren *uvby*, and *JHK* (Cutri et al. 2003) band photometry, which is shown in Fig. 3. Using the PAdova-TRieste Stellar Evolution Code (PARSEC) data base of stellar evolutionary tracks (Bressan et al. 2012), we found the star has a stellar age of 6.9 ± 4.7 Gyr. The error bar is big because K0 dwarfs usually stay on their main sequence for up to 15 Gyr.

4 MCMC FITTING OF RV DATA

In order to quantify the uncertainties of the orbital parameters of the planet, we perform an Markov Chain Monte Carlo (MCMC) analysis using the PYTHON code EMCEE. Our code follows the Bayesian method described in Gregory (2005) and Ford (2005, 2006). Any noise component that cannot be modelled is described by a stellar jitter term $\sigma_{\rm jitter}$ for each corresponding instrument.

Each state in the Markov Chain is described by the parameter set

$$\boldsymbol{\theta} = \{P_{\rm b}, K_{\rm b}, e_{\rm b}, \omega_{\rm b}, M_1, C_{\rm i}, \sigma_{\rm jitter}\}, \quad (1)$$

Table 3. MCMC posteriors for the Keplerian orbital fitting.

Parameter	Credible interval	Maximum likelihood	Units
P_b	42.378 ± 0.01	42.378	d
$T\mathrm{conj}_b$	$5886.76^{+0.62}_{-0.58}$	5886.50	JD
e_b	$0.04^{+0.05}_{-0.03}$	0.02	
ω_b	$2.6^{+2.2}_{-1.4}$	2.2	rad
K_b	$1.81^{+0.10}_{-0.10}$	1.80	m s^{-1}
C_{TOU}	-0.32 ± 0.26	-0.31	m s^{-1}
C_{HIRES}	0.23 ± 0.23	0.24	m s^{-1}
C_{PFS}	-0.37 ± 0.39	-0.38	m s^{-1}
C_{CHIRON}	0.16 ± 0.19	0.16	m s^{-1}
$C_{\mathrm{HARPS_old}}$	0.05 ± 0.09	0.0.04	m s^{-1}
$C_{\mathrm{HARPS_new}}$	-0.02 ± 0.23	-0.02	m s^{-1}
σ_{TOU}	$2.06^{+0.28}_{-0.27}$	2.03	m s^{-1}
σ_{HIRES}	$3.08^{+0.19}_{-0.17}$	3.06	m s^{-1}
σ_{PFS}	$2.82^{+0.32}_{-0.28}$	2.70	m s^{-1}
σ_{CHIRON}	$2.41^{+0.18}_{-0.16}$	2.39	m s^{-1}
$\sigma_{\mathrm{HARPS_old}}$	$1.81^{+0.07}_{-0.6}$	1.80	m s^{-1}
$\sigma_{\mathrm{HARPS_new}}$	$1.91^{+0.19}_{-0.15}$	1.88	m s^{-1}
$m\sin i$	8.47 ± 0.47	8.43	$M_\oplus$

where P_b is orbital periods, K_b is the RV semi-amplitudes, e_b is the orbital eccentricities, ω_b is the arguments of periastron, M_b is the mean anomalies at chosen epoch (τ), C_i is constant velocity offset between the differential RV data from TOU, Keck, PFS, CHIRON, and HARPS and the zero-point of the Keplerian RV model, and σ_{jitter} is the 'jitter' parameter. The jitter parameter describes any excess noise, including both astrophysical noise (e.g. stellar oscillation and stellar spots; Wright 2005), any instrument noise not accounted for in the quoted measurement uncertainties, and systematic RV errors (Ma et al. 2016).

We use standard priors for each parameter (Gregory 2007). The prior is uniform in the logarithm of the orbital period (P_b) from 1 to 1000 d. For K_b and σ_{jitter}, we use a modified Jefferys prior which takes the form of $p(x) = (x + x_o)^{-1}[\log(1 + x_{\max}/x_o]^{-1}$, where $x_o = 0.1$ m s^{-1} and $x_{\max} = 20$ m s^{-1} (Gregory 2005). Prior for e_b is uniform between zero and unity. Priors for ω_b and M_b are uniform between zero and 2π. For C_i, the prior is uniform between $\min(v_i)-50$ m s^{-1} and $\max(v_i)+50$ m s^{-1}, where v_i are the set of RVs obtained from each of the RV instruments. We verified that the chains did not approach the limiting values of P_b, K_b, and σ_{jitter}.

Following Ford (2006), we adopt a likelihood (i.e. conditional probability of making the specified measurements given a particular set of model parameters) of

$$p(v|\boldsymbol{\theta}, M) \propto \prod_k \frac{\exp[-(v_{k,\theta} - v_k)^2/2(\sigma^2_{k,\mathrm{obs}} + \sigma^2_{\mathrm{jitter}})]}{\sqrt{{\sigma_{k,\mathrm{obs}}}^2 + {\sigma_{\mathrm{jitter}}}^2}}, \quad (2)$$

where v_k is the observed RV at time t_k, $v_{k,\theta}$ is the model velocity at time t_k given the model parameters $\boldsymbol{\theta}$, and $\sigma_{k,\mathrm{obs}}$ is the measurement uncertainty for the RV observation at time t_k.

In Table 3, we show the final parameters and uncertainties obtained with our MCMC analysis. We performed a simultaneous fit of the planetary signal and the activity induced RV jitters using the TOU, Keck, PFS, CHIRON, and HARPS data. From the periodogram of the RV data shown in Fig. 4, we find a strong periodic signal around 42 d. The 0.1 per cent significance level shown on this plot is determined after 10 000 bootstrap resampling. In Fig. 5, we show the best Keplerian orbital fit to the RV data which is attributed to the planet candidate HD 26965b. The phase-folded RV curve is shown in Fig. 6. The rms of the residuals is 2.6 m s^{-1}, and we did not find any additional peak with significance above 0.1 per cent from the periodogram of RV residuals. Adopting a stellar mass of 0.78 $M_\odot$, we derived the minimum mass of the planet $m\sin i = 9.7 \pm 1.3 M_\oplus$.

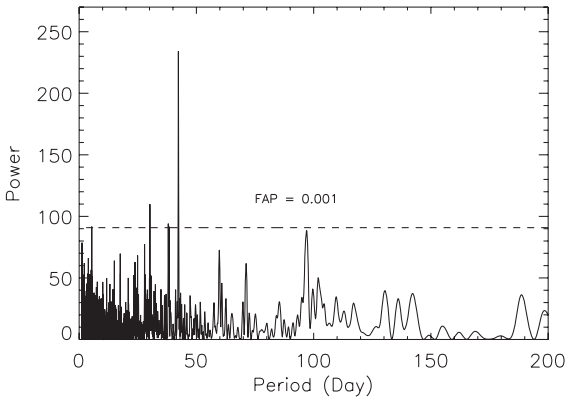

Figure 4. GLS periodogram for the RV data, which clearly shows the peak around 42 d. The horizontal dashed line shows the 0.1 per cent significance level determined using 10 000 bootstrap resamplings and a search window of [2, 200] d.

5 PLANET, OR STELLAR ACTIVITY?

In this section, we discuss the possibility that the RV signal is actually produced by stellar rotation modulated activity (like star-spots, plagues, and convection inhibition; Dumusque et al. 2011). We first determine the possible stellar rotation periods from both stellar activity index and photometric data, and compare them with the period of the RV signal. We then assess the stability of this 42-d RV signal by investigating the evolution of this 42-d RV signal against the number of RV observations. We also discuss the possible RV jitter induced by stellar surface activity and compare it with the amplitude of the 42-d RV signal. Line bisector analysis is conducted in the end to investigate the impact of stellar activity on RV measurements. All of the studies except the activity period in this section support the planet origin of the 42-d RV signal, which are summarized in Table 4.

5.1 Stellar activity index and rotation period

We first determine the rotation period of the star using the stellar activity S index. The S index, calculated from the singly ionized calcium H & K line core emission flux (Wilson 1978), is the most commonly used index of stellar magnetic activity. To put constraints on the rotation period and the magnetic activity cycle of the star, we re-examined the Ca II HK S-index data from Mount Wilson (S_{MW}), HARPS, Keck, and PFS. Olin Wilson's HK Project at the Mount Wilson Observatory (MWO) regularly observed the Ca II HK emission for a sample of over 100 bright dwarf stars beginning in 1966 to characterize magnetic variability of stars other than the Sun (Wilson 1978). We obtained the Mount Wilson data from the National Solar Observatory and present them in Fig. 7. From the plot, we can clearly see a 10.1 yr magnetic cycle (also reported in Baliunas, Sokoloff & Soon 1996), which shows the star periodically enters into an active phase after a relatively quiet phase. Since there is a ~10 yr magnetic cycle, we need to remove its signal first before we can examine the short-term S_{MW} variations caused by stellar rotation. We used a spline function with a breakpoint

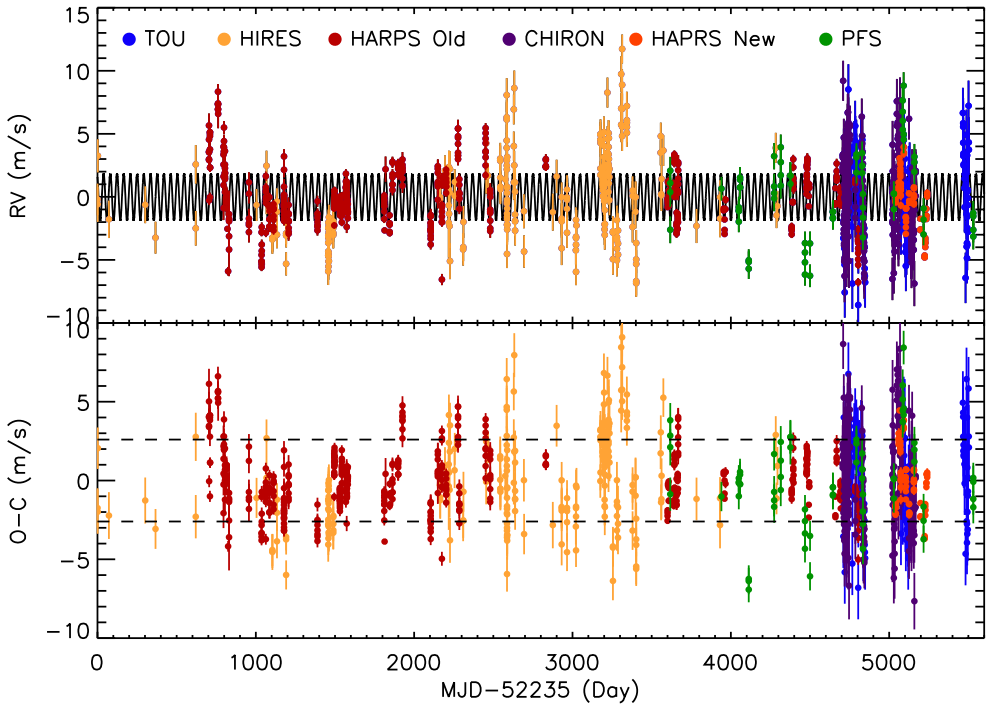

Figure 5. Best-fitting one-planet Keplerian orbital model for HD 26965. The RV data points from Keck/HIRES, HAPRS, PFS, CHIRON, and TOU are shown as yellow, red, and blue dots. The black solid line is the maximum-likelihood model, with the orbital parameters listed in Table 3. The bottom panel shows the RV residuals after subtracting the best-fitting Keplerian RV model. The horizontal dashed lines show the range of the rms value ± 2.6 m s^{-1} .

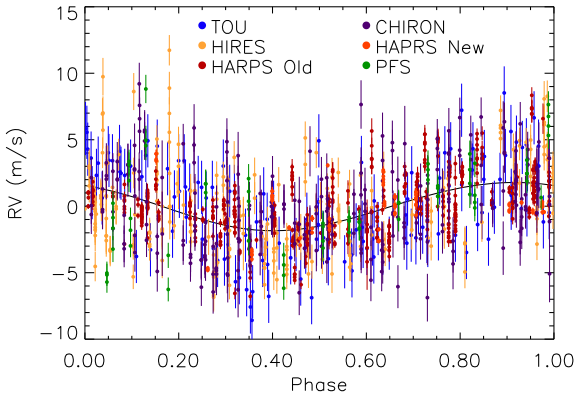

Figure 6. Phase-folded RV curve of HD 26965. The black solid line is best-fitting one-planet Keplerian orbital model, with the orbital parameters listed in Table 3.

of 200 d to de-trend the $S_{\rm MW}$ values. For the S-index data from HAPRS, KECK, and PFS, we use a breakpoint of 500 d because there are not as many data points available as there are from Mount Wilson. After examining the periodogram for the de-trended $S_{\rm MW}$, we do not find a clear peak at 42.4 d. From the study of the Sun, we learn that the active regions are not always concentrated on certain longitudes, hindering the detection of its stellar rotation signal during the active phase. Therefore, we decide to separate these S-index data alternatively into the quiet and active phases as shown in zones 1–9 in Fig. 7 to check for occasionally strong periodic signals.

The periodogram for these marked zones are shown in Fig. 8. We found strong signals in zones 5 and 6, corresponding to an active phase and a quiet phase, respectively. Since the S-index data from HAPRS, KECK, and PFS do not have error bars, we decided to not run periodograms and Sine-curve fitting on these data. The S-index data from zones 5 and 6 together with their best Sine-curve fit are displayed in Fig. 9. HAPRS, Keck, and PFS S-index data from zones 8 and 9 are also displayed in Fig. 9, which support consistent periodic signals found from the Mount Wilson data in both the active and quiet phases. The resulting best-fitting periods for the active and quiet phases are 41.2 ± 0.9 and 39.2 ± 0.7 d, respectively, with errors estimated from the full width at half-maximum (FWHMs) of the peaks in the periodograms. The period variation can be explained by the differential rotation of the star and different locations of active regions similar to our Sun. For comparison, the periodograms of RVs in both the active and quiet phases (Fig. 10) clearly show a stable peak around 42.4 d. The fact that periodograms for the activity indicator $S_{\rm MW}$ show multipeaks, and none of these strong peaks sit exactly at 42.4 d, is an important piece of evidence supporting the planet origin of this 42.4 d signal. The best-fitting amplitudes of the S-index modulation (Fig. 9) are 0.008 and 0.017 in the quiet and the active phases, which demonstrates there is stronger stellar surface activity during the magnetic active phase than during the quiet phase. As explained later in Section 5.4, this finding also supports the planet origin of this 42.4-d signal.

There are several other estimates of the stellar rotation period from previous work, like 43 d using 25 yr of the Ca II HK index measurements from MWO (Baliunas et al. 1996), 42.2 d using the calibrated stellar activity-rotation-age relation (Mamajek & Hillenbrand 2008; Lovis et al. 2011), 43.7 d using the relation from Suárez Mascareño et al. (2015) and Suárez Mascareño, Rebolo & González Hernández (2016). All of the rotation periods estimated above, including our own result, are close to the period of the RV signal detected in this paper, which warrants further discussion of the possibility that this RV signal is induced by stellar surface magnetic activity.

Table 4. Summary of evidence supporting planet origin or stellar activity origin of the detected 42-d RV signal.

Evidence	Planet or Activity origin
$P_{\rm rotation}$ close to 42 d	Activity
Sharp 42-d peak from RV periodogram	Planet
No clear 42-d peak from $S_{\rm MW}$ periodogram	Planet
Clear 42-d peak from magnetic quiet phase RV periodogram	Planet
Clear 42-d peak from magnetic active phase RV periodogram	Planet
Strong 39-d signal from $S_{\rm MW}$ in magnetic quiet phase	Planet
Strong 41-d signal from $S_{\rm MW}$ in magnetic active phase	Planet
No 42-d peak from 23 yr high-precision photometric campaign	Planet
Star-spots $K_{\rm spot} < 0.3$ m s^{-1} from simulation	Planet
Inhibition of convection $K_{\rm inh} < 0.3$ m s^{-1} from linear interpolation	Planet
Active phase and quiet phase have similar K values detected	Planet
No strong correlation between RV and BIS	Planet

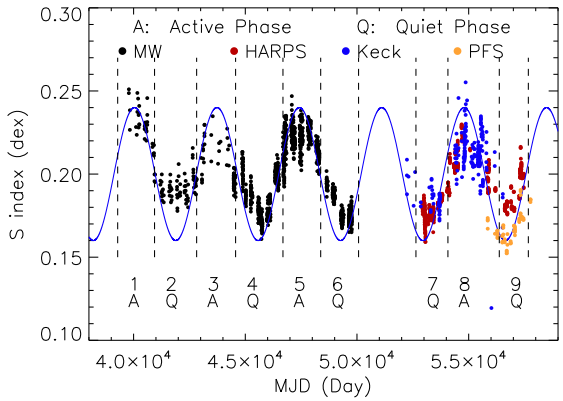

Figure 7. Measurements of Ca II HK S index of HD 26965. The data are collected from MWO (black), HARPS (red), Keck (blue), and PFS (orange). We overplotted a Sine curve with a 10.1 yr period to show the sun-like magnetic cycle. The data are separated into alternative magnetic quiet and active phases, which are marked by a zone number from 1 to 9. In the plot, 'A' represents magnetic active phase, and 'Q' represents magnetic quiet phase.

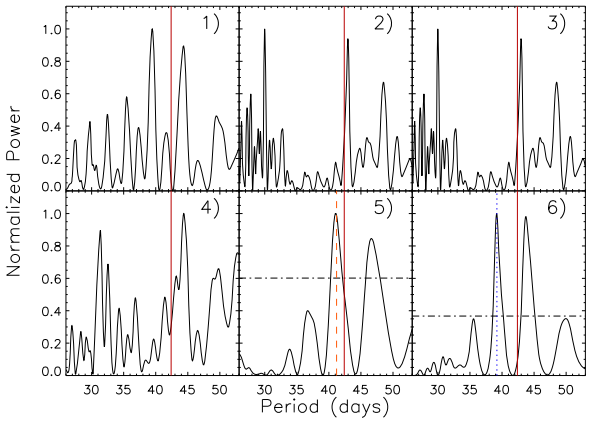

Figure 8. Periodograms for the Mount Wilson Ca II HK S index. From top left to bottom right, the panels show periodograms of $S_{\rm MW}$ from zones 1 to 6 marked as in Fig. 7. We searched for strong periodic signals around 42 d in each zone. The horizontal dashed lines shown in panels 5 and 6 mark the 0.1 per cent significance level, which is derived using 10 000 times bootstrap resampling and a search window of [2, 300] d. The red vertical solid line in each panel shows the period of the planet candidate HD 26965b at 42.4 d. The orange vertical dashed line in panel 5 shows the period of a strong signal in a magnetic active phase at 41.2d. The blue dotted vertical line in panel 6 shows the period of the strong signal in a magnetic quiet phase at 39.2d.

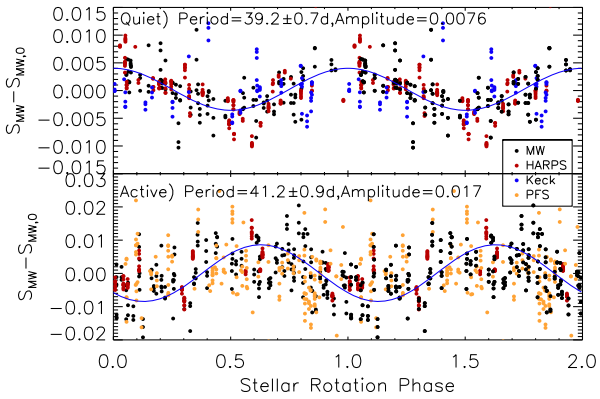

Figure 9. Phase-folded Mount Wilson, HAPRS, Keck, and PFS S index measurements of HD 26965. The data shown in the top panel are from the magnetic quiet phase, and the data in the bottom panel are from the magnetic active phase. We fitted a Sine function to the S index after subtracting their median value, and calculated the best-fitting period and amplitude for both phases using the Mount Wilson data. The S indices from HARPS, Keck, and PFS were not used in the Sine-curve fitting, but they are consistent with the rotation period fitted from the Mount Wilson data. The active phase shows a bigger S index variation amplitude due to a more active status of the star compared to the quiet phase.

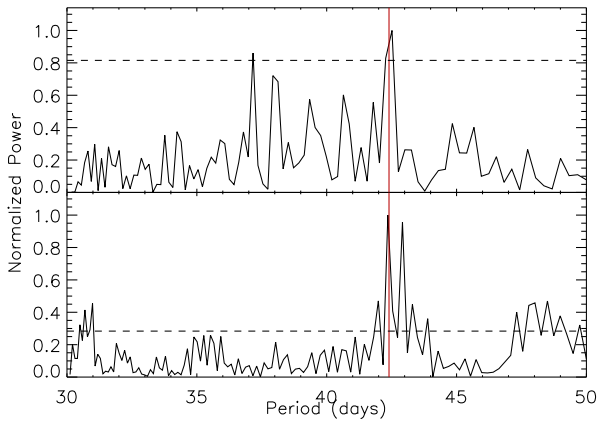

Figure 10. Periodograms for the RVs for alternating active (the top panel) and quiet phases (the bottom panel), respectively. Both periodograms show a clear peak around 42.4 d, which is marked with a vertical red solid line. The horizontal dashed line in each panel marks the 1 per cent significance level, which is derived using a 1000 times bootstrap resampling and a search window of [2, 300] d.

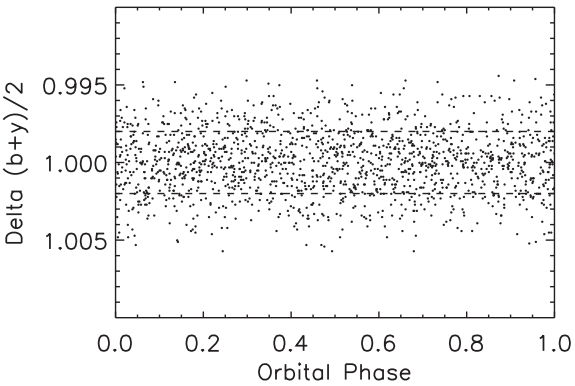

Figure 11. Photometric data of HD 26965 acquired with the T4 APT at Fairborn Observatory from 1993 to 2017. A total of 1550 differential photometric data points of HD 26965 are phased to the period of the planet RV signal. The two horizontal dashed line correspond to the $\pm 1\sigma$ range of the brightness level of the 1550 observations.

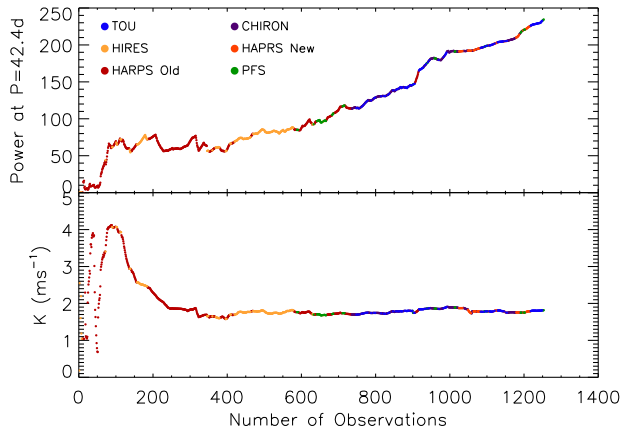

Figure 12. Periodogram of photometric data for HD 26965 from Fairborn. There is no significant peak except the 1-d alias in the top panel. The double red solid lines mark the region around $P = 42.38$ d, which is the planet orbital period. In the second, third and fourth panels, we inject a periodic signal at semi-amplitudes of 0.0003, 0.0004, and 0.0005 mag to the original photometric data. The peak at 42 d becomes higher as the injected signal becomes stronger. Comparing the simulated periodogram with the original periodogram in the top panel, we can rule out a periodic signal stronger than 0.0004 mag. We note here that the 1 yr alias of the 42.4 d signal, which sits at 38 d, also becomes stronger.

5.2 Photometric results and rotation period

In this section, we search for a periodic rotation signal from photometric data. In Fig. 11, we plot all 1550 photometric measurements from Fairborn Observatory plotted against the orbital phase of HD 26965b with $P_b = 42.38$ d. The standard deviation of these data from their mean is 0.002 mag. A least-squares Sine-curve fit to the phased data gives a full amplitude of 0.0000 ± 0.0002 mag. We can rule out a sinusoidal brightness variation larger than 0.0006 mag at 3σ confidence at the orbital period of the planet candidate. To put further constraint on the upper limit of a detectable periodic photometric signal that might be induced by star-spots, we did a simple simulation by adding a sinusoidal photometric signal to the photometric data collected from Fairborn. The period for this signal is set to be the same as the period of the planet signal ($P = 42.38$ d), and the semi-amplitude is chosen to be 0.0003, 0.0004, and 0.0005 mag. From the periodogram shown in Fig. 12, we cannot detect the

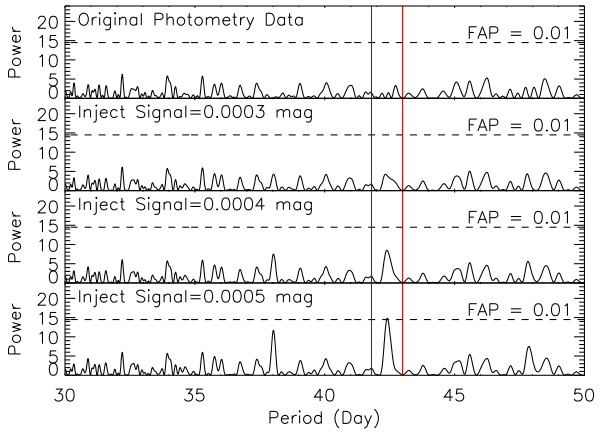

Figure 13. Evolution of the significance of the detected signal and its semi-amplitude as a function of the number of measurements. The semi-amplitude is derived using a fixed orbital period and eccentricity.

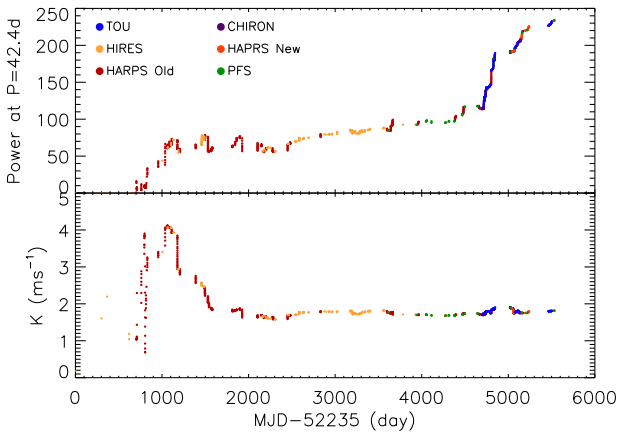

Figure 14. Evolution of the significance of the detected signal and its semi-amplitude as a function of the date of the observations. The semi-amplitude is derived using a fixed orbital period and eccentricity.

0.0002 mag signal, but can start to detect this periodic photometric signal at 0.0005 mag. This simulation helps rule out a detectable periodic photometric signal with a semi-amplitude larger than 0.0004 mag. We use this information to put a constraint on stellar RV jitters induced by star-spot activity in the next section.

5.3 RV signal evolution

To assess the stability of this RV signal, we study the evolution of this 42-d RV signal against the number of observations and date of observations in this section. The significance power of this 42-d signal is calculated using a generalized Lomb–Scargle periodogram (GLS) following Zechmeister & Kürster (2009). Fig. 13 shows the evolution of the signal significance and its velocity semi-amplitude (K) against number of observations. The evolution of this 42-d signal is steady and continuous after $N = 400$ data points. Fig. 14 shows the evolution of the signal significance and its velocity semi-amplitude (K) against the date of observation. By studying the evolution against the date of observations, we can also see the importance of the high-cadence Dharma survey observations. The slope of the significance increased after the start of the TOU nightly cadence campaigns in 2015, which means that the time needed for the detection of short-period planets decreases significantly, similar

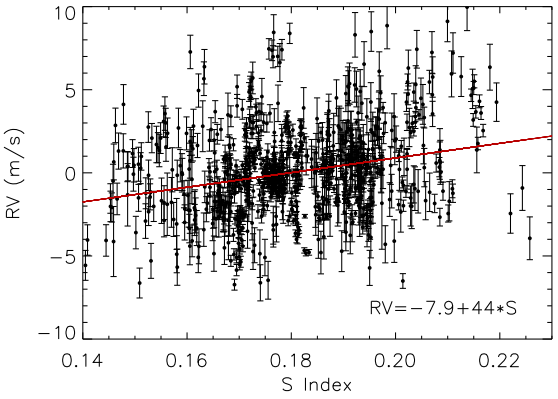

Figure 15. Correlation between Ca II HK S index and RV measured by HARPS, HIRES, and PFS. The red solid line shows the best linear-fitting result (RV = $-7.9 + 44 \times S$).

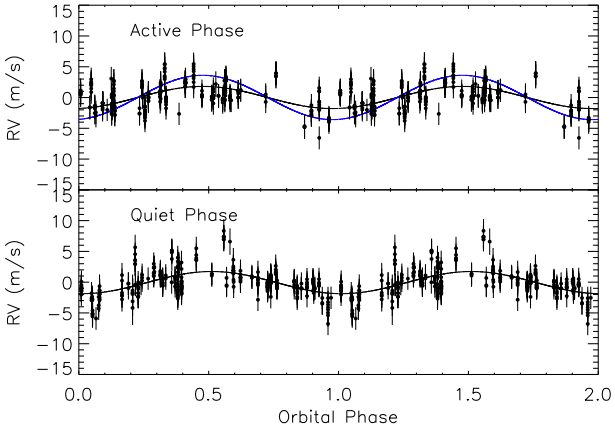

Figure 16. RV data from HARPS, which are divided into quiet (bottom panel) and active (top panel) phases according to the magnetic cycle of the star. We use $P = 42.38$ d and $e = 0$ to fit the RV data to study the RV amplitude variation from the quiet to active phases. The black lines in both panels show the best-fitting RV models, and the blue solid line in the top panel shows a model with an RV amplitude two times of that from the quiet phase. The fitting result does not support the hypothesis that the RV amplitude in the active phase became twice as large as that in the quiet phase, which supports the planet origin of the 42-d RV signal.

to what happened with the discovery of Proxima b (Anglada-Escudé et al. 2016). If this 42-d RV signal is generated by stellar activity, it should not be so stable given the large-amplitude variation of stellar activity strength from its magnetic cycle. These two plots support the stableness of the orbital parameters and, thus, the planetary source of this 42-d RV signal (Suárez Mascareño et al. 2017a).

5.4 Stellar activity RV Jitter

In this section, we provide additional evidence to support the planet nature of this RV signal. There are several stellar activity sources that can generate an RV signal detected in this paper, like dark spots, plages, and convection inhibition (Vanderburg et al. 2016). We discuss these possibilities in this section. First, we simulated the RV signal induced by dark spots using a modified code of SOAP2.0 (Spot Oscillation And Planet, Dumusque, Boisse & Santos 2014; Kimock et al., in preparation). By setting a photometric variation semi-amplitude of 0.0004 mag, the upper limit derived from the last section, and using a single-spot model for simplicity, the maximum RV signal generated has $K_{\rm spot} < 0.3$ m s^{-1}, which is a factor of seven times less than the RV signal detected. We also explored a more realistic multispot model similar to the Sun in our simulation; the RV signal generated is even smaller in the $K_{\rm spot}$ value, similar to what was concluded in the previous study by Dumusque et al. (2014).

Secondly, the inhibition of convection due to surface magnetic activity can generate artificial redshift. Solar-like magnetic cycles are characterized by an increasing filling factor of active regions when the activity level increases. Because convection is strongly reduced in active regions as a result of the magnetic field, the star appears redder (thus positive RV) during its high-activity phase. A positive correlation between the RVs and the activity level is therefore observed (Meunier, Lagrange & Desort 2010). However, neither Santos et al. (2010) nor Lovis et al. (2011) found any significant RV variation from HD 26965 due to convection inhibition during its magnetic cycle (<2 m s^{-1}). Here, we reproduced this correlation in Fig. 15 using the RV and Ca II HK S-indices data from HARPS, PFS, and Keck/HIRES, and made a linear fit to this correlation. We came to the same conclusion as stated by Santos et al. (2010), that there is a very weak correlation between the RV and Ca II HK S-index. Using the linear relation from Fig. 15, the convection inhibition can generate an RV variation with a semi-amplitude $K_{\rm inh} \sim 0.2$ m s^{-1} within a 42-d period when the periodic coherent Ca II HK S-index variation is as small as ∼0.004 (semi-amplitude) shown in the top panel of Fig. 9. Clearly, this is not big enough to explain the semi-amplitude of ∼1.8 m s^{-1} RV signal detected.

The above discussions show that the most common types of magnetic activity cannot induce the RV signal detected in this investigation. Next, we present additional evidence against the activity origin of this 42-d RV signal. In the previous section, we identified the magnetic active phases and quiet phases based on over 30 yr of Ca II HK index measurements of HD 26965 (Fig. 7). We then divided all the RV measurements into either an active phase or a quiet phase. The phased curves of Ca II HK index measurements in Fig. 9 show that the surface activity filling factor varies a factor of two between the quiet phase and the active phase. Lanza et al. (2016) found there is a positive correlation between solar RV variation and the level of chromospheric activity measured using Ca II HK index. If the coherent 42-d RV signal detected is from stellar activity modulated by the rotation, we expect the RV amplitude would become two times larger in the active phase than in the quiet phase because the coherent S-index variation in the active phase is twice as large as that in the quiet phase. Since HARPS RV data span over more than 10 yr, we choose to use HARPS RV data to test this scenario. After dividing HAPRS RV data into active- and quiet-phase data, we did a Keplerian RV fitting for each phase. During the fitting, we fixed two parameters with $P = 42.38$ d and $e = 0.0$ to focus on the velocity semi-amplitude variation. The fitting results are shown in Fig. 16, with $K_{\rm active} = 1.7 \pm 0.3$ m s^{-1} and $K_{\rm quiet} = 1.8 \pm 0.4$ m s^{-1}. The fact that RV amplitude does not increase significantly from the quiet phase to the active phase again supports the planet origin of this 42-d RV signal.

In Suárez Mascareño et al. (2017b), they studied the RV signal induced by stellar activity and rotation among 55 late-type dwarf stars using HARPS data. They derived an empirical relationship between the mean level of chromospheric emission and the RV semi-amplitude shown in fig. 9 of their paper. Using $\log(R'_{\rm HK}) = -4.99$ from Jenkins et al. (2011), we estimate that the expected RV signal at this level of stellar activity is ∼0.35 m s^{-1}, which is much smaller

than the stable $\sim$1.8 m s^{-1} RV signal detected. This also supports the planet origin of this 42-d RV signal.

Vanderburg et al. (2016) conducted extensive sets of simulations to study the impact of stellar surface activity modulated by stellar rotation on the ability to detect planets using the RV technique. In their simulations, they usually assume RV observations with ideal sampling, which is similar to the situation in this paper when combining the Keck/HIRES, HARPS, PFS, CHIRON, and TOU observations. They found that an activity signal identified from the RV periodogram at a period of $P_{\rm activity}$ usually has a width as large as $\sim 0.1 * P_{\rm activity}$ because of the lifetime of spots and differential stellar rotation. While in our RV periodogram, the peak at 42 d is very sharp with an FWHM = 0.3 d. This points to the likely conclusion that the coherent 42-d RV signal found from HD 26965 is induced by a planet, not magnetic activity.

5.5 Line bisector analysis

Line bisector analysis is another diagnostic tool to investigate the possible impact of stellar activity on RV measurements (Toner & Gray 1988; Queloz et al. 2001; Wright et al. 2013). Here, we performed a correlation study of the Bisector Inverse Slope (BIS) and the RVs from the fibre-fed TOU spectrograph. In our RV data pipeline, we do not use the cross-correlation function (CCF) method employed by HARPS (Ma & Ge, in preparation). Instead we use a template matching method similar to Zechmeister et al. (2018). Thus, we do not have a traditional CCF product from our pipeline to calculate the BIS. Instead, we used the reduced-χ^2 function from our template matching pipeline to calculate the BIS. Similar to the method employed by Santos et al. (2002) on their analysis of the HARPS CCF, we compute the bisector velocity for 10 different levels on the reduced-χ^2 function from TOU. The BIS is calculated by averaging the upper and lower bisector points before subtracting one from the other. Here, we choose the definition from Queloz et al. (2001) where they use the 10–40 per cent and 55–85 per cent CCF depth (see also Wright et al. 2013). This quantity is equivalent to the BIS from the CCF method since both trace the asymmetry in the absorption line profile variation caused by stellar surface activity. The Spearman's rank correlation coefficient between the RV and the BIS is 0.15 with a significance level of 0.08, which suggests there does not exist a strong correlation between the RV and BIS. This is more strong evidence to argue against the activity origin of the 42-d RV signal.

6 CONCLUSION AND DISCUSSION

In a search through the early RV data from the DPS survey, we discovered an RV signal consistent with a super-Earth orbiting a V = 4.4 K dwarf, HD 26965. Additional RV data were found from the Keck archive and HARPS archive. After combining the RV data from the DPS survey with data from Keck/HIRES and HAPRS, we use an MCMC code to find the best-fitting orbital parameters with an orbital period of 42.38 $\pm$ 0.01 d, eccentricity of $0.04^{+0.05}_{-0.03}$, and velocity semi-amplitude of 1.81 $\pm$ 0.10 m s^{-1} . Adopting a stellar mass of 0.78 $M_\odot$ for HD 26965, the minimum mass for the planet is 8.47 $\pm$ 0.47 Earth masses, which puts it in the super-Earth mass range.

The 42-d period RV signal has also been reported in Díaz et al. (2018). We privately communicated about our discoveries during the 2017 summer extremely precise RV meeting at the Pennsylvania State University. The best Keplerian solution reported from their modelling has a $P = 42.364 \pm 0.015$ d, $e = 0.017 \pm 0.046$, and $K = 1.59 \pm 0.15$ m s^{-1} . The periods reported from our paper and their paper are similar. The fact they reported a smaller RV signal may be related to their modelling of red noise and linear correlations with stellar activity indicators, in addition to the white noise used in our RV modelling.

The conclusion from Díaz et al. (2018) is that the RV signal can be either from a planet or from stellar activity. Using Ca II HK index variation, we find this star does show a long-term magnetic cycle of $\sim$10.1 yr. The fact that the orbital period of the planet is close to the rotation period of the star is concerning, because stellar rotation modulation of magnetic activity can mimic planet signals (Saar & Donahue 1997; Desort et al. 2007; Ma & Ge 2012). For instance, Queloz et al. (2001) found that the RV variation of a G0V star, HD 166435, is from surface spot activity, not a planet. Huélamo et al. (2008) and Huerta et al. (2008) also found that two previously claimed exoplanets are actually caused by star-spots on the stellar surface. Mahmud et al. (2011) showed that cool surface spots could cause the periodic RV variability on a T Tauri star.

By carefully examining the RV data in the active and quiet phases of the star, and after carefully considering all possible stellar activity sources, we concluded that the coherent signal seen from HD 26965 is most likely from a planet, with some RV noise contributed by stellar activity. In addition, the sharpness of the 42-d peak in the RV periodogram also supports the planet origin of the 42-d RV signal as active regions on the stellar surface modulated by differential rotation of the star normally reveal themselves as a group of peaks around the mean rotation period (Vanderburg et al. 2016). The evolution of the RV semi-amplitude to a stable value after several years of observations provides additional strong support for the planet origin of this 42-d RV signal. Our high-quality photometric data set helps rule out any significant photometric variation at 42 d. This also supports the planet origin of this 42-d RV signal. This plethora of evidence allows us to draw the conclusion that this 42-d RV signal is from a planet, unlike the uncertainties reported in Díaz et al. (2018).

Currently, there are several planet systems known to host planets with periods close to the rotation period of the star (Dragomir et al. 2012; Haywood et al. 2014), or close to the magnetic cycle period of the star (Wright et al. 2008; Kane et al. 2016). For example, Dragomir et al. (2012) found a Jupiter-mass planet orbiting HD 192263 with a period of 24.4 d using RV from Keck/HIRES and CORALIE, and derived a stellar rotation period of 23.4 d using photometric data. We note here that Henry, Donahue & Baliunas (2002) initially suggested that the RV signal around HD 192263 is caused by rotational modulation of surface activity. But Santos et al. (2003) used significant changes of photometric patterns over time and 3 yr of coherent RV observations to prove that the signal is indeed from a planet. In the case of HD 26965, we cannot derive a precise stellar rotation period because our ground-based photometric data did not reveal any significant periodic variation around 42 d. Future high-precision space photometric observations can help detect possible small photometric variation from the star (<400 ppm) caused by the surface spots. As pointed out by Vanderburg et al. (2016), it is very important for next generation RV planet surveys to have simultaneous photometric observations for measuring rotation periods and activity signals. Our data analysis also demonstrates the importance of having simultaneous photometry for the purpose of disentangling planet signals from magnetic activity signals.

HD 26965 is a very bright metal poor star with $V = 4.4$. This makes it the second brightest star in the night sky with a super-Earth detection so far, just behind HD 20794 ($V = 4.3$, Pepe et al. 2011).

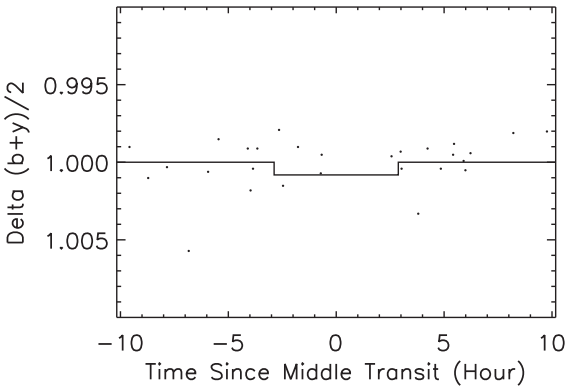

Figure 17. Phased photometric data of HD 26965 from Fairborn Observatory. It is an expanded version of Fig. 11. This figure is centred on the predicted middle transit time. The solid curve shows the predicted central transit signal with a depth of 0.0008 mag. The current data do not support the existence of a transit signal.

One interesting fact is that HD 20794 has a similar metallically (Fe/H $= -0.4 \pm 0.1$) as that of HD 26965 (Fe/H $= -0.42 \pm 0.04$), which is consistent with the finding of Petigura et al. (2018) that smaller planets are detected around stars with wide-ranging metallicities.

Based on the observed properties of HD 26965 b, several inferences of the planet's properties and history are possible. With a minimum mass of $8.4M_{\oplus}$, the planet likely possesses a gaseous atmosphere based on other planets with known masses and radii (Rogers 2015). However, we note that Kepler-10 c has a similar mass and orbit, is hosted by a similar, low-metallicity star (Batalha et al. 2011; Fressin et al. 2011; Weiss et al. 2016; Rajpaul, Buchhave & Aigrain 2017), and does not possess an envelope (Lopez & Fortney 2014), so HD 26965 b may be a similar type of world. In the near-term, this possibility can only be resolved if a transit is detected.

Detecting exoplanets via the RV technique and subsequently monitoring their transit windows is one of the most fruitful strategies for finding bright stars with transiting planets, which are the best candidates for exoplanet atmospheric studies. Fig. 17 shows the photometric data near the predicted middle transit time. The expected duration of a central transit is $\sim R_{\star}P/(\pi a) = 5.8$ h, and the expected depth is $(R_b/R_{\star})^2 \sim 0.0008$. Our current photometric data do not support the existence of a shallow transit from HD 26965b.

Lastly, the detection of HD 26965b shows the advantage of the DPS strategy. The high precision and high cadence RV campaign from TOU have greatly increased the detection sensitivity of low-mass planets. The fact that we can discover this system with similar RV precision to HAPRS (Ma & Ge, in preparation), but with high cadence (133 nights observations within 2 yr using TOU versus 97 nights observations within 13 yr using HARPS), demonstrates that high-precision and high-cadence RV surveys of bright stars in the solar neighbourhood will likely lead to the detection of a large number of low-mass planets with high completeness, and possible detections of low-mass planets in their habitable zones (Ge et al. 2016).

ACKNOWLEDGEMENTS

We thank the anonymous referee for comments and suggestions which have helped significantly improve the quality of this paper. We are grateful to the Dharma Endowment Foundation for generous support. We thank Indiana University for the donation of their 50-inch telescope to the Department of Astronomy, University of Florida. BM thanks the support of the National Aeronautics and Space Admistration (NASA)-WIYN observation award. JIGH acknowledges financial support from the Spanish Ministry of Economy and Competitiveness (MINECO) under the 2013 Ramón y Cajal program MINECO RYC-2013-14875, and the Spanish ministry project MINECO AYA2014-56359-P. We are grateful to Lou Boyd of Fairborn Observatory, and engineering staff at Steward Observatory, Bruce Hille, Scott Swindell, Joe Horscheidt, Melanie Waidanz, Chris Johnson, and Jeff Kingsley for providing excellent engineering support for the DPS. This paper is dedicated to the memory of the wonderful technical manager of Steward Observatory, Mr. Robert Peterson, who helped get the Dharma Endowment Foundation Telescope (DEFT) project going on Mt. Lemmon in 2015–2016 before he passed away on 2016 October 20. GWH acknowledges long-term support from NASA, National Science Foundation (NSF), Tennessee State University, and the State of Tennessee through its Centers of Excellence program.

REFERENCES

Anglada-Escudé G. et al., 2016, Nature, 536, 437
Baliunas S. L. et al., 1995, ApJ, 438, 269
Baliunas S., Sokoloff D., Soon W., 1996, ApJ, 457, L99
Batalha N. M. et al., 2011, ApJ, 729, 27
Batalha N. M. et al., 2013, ApJS, 204, 24
Bonfils X. et al., 2013, A&A, 549, A109
Borgniet S., Lagrange A.-M., Meunier N., Galland F., 2017, A&A, 599, A57
Bressan A., Marigo P., Girardi L., Salasnich B., Dal Cero C., Rubele S., Nanni A., 2012, MNRAS, 427, 127
Brewer J. M., Giguere M., Fischer D. A., 2014, PASP, 126, 48
Buchhave L. A. et al., 2016, AJ, 152, 160
Burke C. J. et al., 2015, ApJ, 809, 8
Butler R. P., Marcy G. W., Williams E., McCarthy C., Dosanjh P., Vogt S. S., 1996, PASP, 108, 500
Butler R. P. et al., 2017, AJ, 153, 208
Christiansen J. L. et al., 2016, ApJ, 828, 99
Coughlin J. L. et al., 2016, ApJS, 224, 12
Crane J. D., et al., 2010, Proc. SPIE, 7735, 773553
Cutri R. M. et al., 2003, yCat, 2246, 0
Delgado Mena E., Tsantaki M., Adibekyan V. Z., Sousa S. G., Santos N. C., González Hernández J. I., Israelian G., 2017, A&A, 606, A94
Desort M., Lagrange A.-M., Galland F., Udry S., Mayor M., 2007, A&A, 473, 983
Díaz M. R. et al., 2018, AJ, 155, 126
Dragomir D. et al., 2012, ApJ, 754, 37
Dressing C. D., Charbonneau D., 2015, ApJ, 807, 45
Ducati J. R., 2002, yCat, 2237, 0
Dumusque X., Udry S., Lovis C., Santos N. C., Monteiro M. J. P. F. G., 2011, A&A, 525, A140
Dumusque X. et al., 2012, Nature, 491, 207
Dumusque X., Boisse I., Santos N. C., 2014, ApJ, 796, 132
Eaton J. A., Henry G. W., Fekel F. C., 2003, in Oswalt T. D., ed., The Future of Small Telescopes in the New Millennium, Vol. II, The Telescopes We Use. Kluwer, Dordrecht, p. 189
Ford E. B., 2005, AJ, 129, 1706
Ford E. B., 2006, ApJ, 642, 505
Foreman-Mackey D., Hogg D. W., Morton T. D., 2014, ApJ, 795, 64
Fressin F. et al., 2011, ApJS, 197, 5
Fressin F. et al., 2013, ApJ, 766, 81
Ge J. et al., 2012, Proc. SPIE, 8446, 84468R
Ge J. et al., 2014, Proc. SPIE, 9147, 914786
Ge J. et al., 2016, Proc. SPIE, 9908, 99086I
Gregory P. C., 2005, ApJ, 631, 1198
Gregory P. C., 2007, MNRAS, 381, 1607

Haywood R. D. et al., 2014, MNRAS, 443, 2517
Heintz W. D., 1974, AJ, 79, 819
Henry G. W., 1995a, in Henry G. W., Eaton J. A., eds, ASP Conf. Ser., Vol. 79, Robotic Telescopes: Current Capabilities, Present Developments, and Future Prospects for Automated Astronomy. Astron. Soc. Pac., San Francisco, p. 37
Henry G. W., 1995b, in Henry G. W., Eaton J. A., eds, ASP Conf. Ser., Vol. 79, Robotic Telescopes: Current Capabilities, Present Developments, and Future Prospects for Automated Astronomy. Astron. Soc. Pac., San Francisco, p. 44
Henry G. W., Franz O. G., Wasserman L. H., Benedict G. F., Shelus P. J., Ianna P. A., Kirkpatrick J. D., McCarthy D. W. Jr., 1999, ApJ, 512, 864
Henry G. W., Donahue R. A., Baliunas S. L., 2002, ApJ, 577, L111
Howard A. W. et al., 2010, ApJ, 721, 1467
Howard A. W. et al., 2012, ApJS, 201, 15
Huélamo N. et al., 2008, A&A, 489, L9
Huerta M., Johns-Krull C. M., Prato L., Hartigan P., Jaffe D. T., 2008, ApJ, 678, 472
Jenkins J. S. et al., 2011, A&A, 531, A8
Kane S. R. et al., 2016, ApJ, 820, L5
Kang W., Lee S.-G., 2012, MNRAS, 425, 3162
Kurucz R., 1993a, ATLAS9 Stellar Atmosphere Programs and 2 km/s grid. Kurucz CD-ROM No. 13. Smithsonian Astrophysical Observatory, Cambridge, MA, p. 13
Lanza A. F., Molaro P., Monaco L., Haywood R. D., 2016, A&A, 587, A103
Lopez E. D., Fortney J. J., 2014, ApJ, 792, 1
Lovis C. et al., 2011, preprint (arXiv:1107.5325)
Ma B., Ge J., 2012, ApJ, 750, 172
Ma B. et al., 2016, AJ, 152, 112
Mahmud N. I., Crockett C. J., Johns-Krull C. M., Prato L., Hartigan P. M., Jaffe D. T., Beichman C. A., 2011, ApJ, 736, 123
Mamajek E. E., Hillenbrand L. A., 2008, ApJ, 687, 1264
Mayor M. et al., 2003, The Messenger, 114, 20
Mayor M. et al., 2009, A&A, 507, 487
Mayor M. et al., 2011, preprint (arXiv:1109.2497)
Meunier N., Lagrange A.-M., Desort M., 2010, A&A, 519, A66
Morton T. D., Bryson S. T., Coughlin J. L., Rowe J. F., Ravichandran G., Petigura E. A., Haas M. R., Batalha N. M., 2016, ApJ, 822, 86
Motalebi F. et al., 2015, A&A, 584, A72
Mulders G. D., Pascucci I., Apai D., 2015, ApJ, 798, 112
Mullally F. et al., 2015, ApJS, 217, 31
Pepe F. et al., 2011, A&A, 534, A58
Perger M. et al., 2017, A&A, 598, A26
Petigura E. A., Marcy G. W., Howard A. W., 2013, ApJ, 770, 69
Petigura E. A., , et al., 2018, AJ, 155, 89
Queloz D. et al., 2001, A&A, 379, 279
Rajpaul V., Buchhave L. A., Aigrain S., 2017, MNRAS, 471, L125
Rivera E. J., Butler R. P., Vogt S. S., Laughlin G., Henry G. W., Meschiari S., 2010, ApJ, 708, 1492
Rogers L. A., 2015, ApJ, 801, 41
Saar S. H., Donahue R. A., 1997, ApJ, 485, 319
Santerne A. et al., 2016, A&A, 587, A64
Santos N. C. et al., 2002, A&A, 392, 215
Santos N. C. et al., 2003, A&A, 406, 373
Santos N. C., Gomes da Silva J., Lovis C., Melo C., 2010, A&A, 511, A54
Sneden C. A., 1973, PhD thesis, Dissertation Abstracts International
Suárez Mascareño A., Rebolo R., González Hernández J. I., Esposito M., 2015, MNRAS, 452, 2745
Suárez Mascareño A., Rebolo R., González Hernández J. I., 2016, A&A, 595, A12
Suárez Mascareño A. et al., 2017a, A&A, 612, A41
Suárez Mascareño A., Rebolo R., González Hernández J. I., Esposito M., 2017b, MNRAS, 468, 4772
Tabernero H. M., Montes D., González Hernández J. I., 2012, A&A, 547, A13
Tokovinin A., Fischer D. A., Bonati M., Giguere M. J., Moore P., Schwab C., Spronck J. F. P., Szymkowiak A., 2013, PASP, 125, 1336
Toner C. G., Gray D. F., 1988, ApJ, 334, 1008
Torres G., Andersen J., Giménez A., 2010, A&AR, 18, 67
Tsantaki M., Sousa S. G., Adibekyan V. Z., Santos N. C., Mortier A., Israelian G., 2013, A&A, 555, A150
Vanderburg A., Plavchan P., Johnson J. A., Ciardi D. R., Swift J., Kane S. R., 2016, MNRAS, 459, 3565
Vogt S. S., , et al., 1994, Proc. SPIE, 2198, 362
Vogt S. S., Butler R. P., Rivera E. J., Haghighipour N., Henry G. W., Williamson M. H., 2010, ApJ, 723, 954
Vogt S. S. et al., 2015, ApJ, 814, 12
Weiss L. M., , et al., 2016, ApJ, 819, 83
Wilson O. C., 1978, ApJ, 226, 379
Wright J. T., 2005, PASP, 117, 657
Wright J. T., Marcy G. W., Butler R. P., Vogt S. S., Henry G. W., Isaacson H., Howard A. W., 2008, ApJ, 683, L63
Wright J. T. et al., 2013, ApJ, 770, 119
Zechmeister M., Kürster M., 2009, A&A, 496, 577
Zechmeister M. et al., 2018, A&A, 609, A12

SUPPORTING INFORMATION

Supplementary data are available at *MNRAS* online.

Table 1. RV measurements of HD 26965 from TOU.

Please note: Oxford University Press is not responsible for the content or functionality of any supporting materials supplied by the authors. Any queries (other than missing material) should be directed to the corresponding author for the article.

This paper has been typeset from a TEX/LATEX file prepared by the author.